RSC Advances

ROYAL SOCIETY
OF CHEMISTRY

www.rsc.org/advances

Red-Emission Enhancement of the CaAlSiN$_3$:Eu^{2+} Phosphor by Partial Substitution for Ca$_3$N$_2$ by CaCO$_3$ and Excessive Calcium Source Addition

ShuXing Li[1,2], XueJian Liu[1,*], RiHua Mao[3], ZhengRen Huang[1], RongJun Xie[4,*]

[1]The State Key Lab of High Performance Ceramics and Superfine Microstructure, Shanghai Institute of Ceramics, Chinese Academy of Science, Shanghai 200050, China

[2]University of Chinese Academy of Sciences, Beijing 100049, China

[3]Analysis and Testing Center for Inorganic Materials, Shanghai Institute of Ceramics, Chinese Academy of Science, Shanghai 200050, China

[4]National Institute for Materials Science (NIMS), Namiki 1-1, Tsukuba, Ibaraki 305-0044, Japan

*Correspondence Authors:

X. Liu: email, xjliu@mail.sic.ac.cn; Tel., +86-21-52414220.

R. Xie: email, XIE.Rong-Jun@nims.go.jp; Tel., +81-29-860-4312.

Abstract

The effects of different calcium sources and the non-stoichiometric calcium addition on the preparation and photoluminescence properties of the red-emitting nitride phosphor CaAlSiN$_3$:Eu^{2+} were studied. Better crystallinity, enhanced emission intensity, and improved photoluminescence thermal stability of the phosphors were obtained when 10% of the calcium source (Ca$_3$N$_2$) was substituted by CaCO$_3$. The partial substitution for Ca$_3$N$_2$ by CaCO$_3$ resulted in the formation of more transient liquid phases at high temperature, which suppressed the evaporation of Ca/Eu elements to some extent. In order to effectively compensate for the calcium deficiency, excessive initial Ca source was added, resulting in narrower emission band and faster decay rate. Furthermore, the as-synthesized CaAlSiN$_3$:Eu^{2+} was employed as red-emitting component to fabricate

the two-phosphor-converted white LEDs, which exhibited high color rendering index R_a of ~ 98 and warm correlated color temperature of 3000 K, and the narrower emission band with 140 % initial Ca content gave an increase of 15% in luminous efficiency.

Key words: Transient liquid phase; Narrow emission band; Decay behavior; High-color-rendition white LED

1 Introduction

Recently, considerable efforts have been devoted to the development of nitride phosphors for application in white light-emitting diodes (LED). $CaAlSiN_3:Eu^{2+}$ has been known as an excellent red-emitting phosphor for high-color-rendition white LED due to its adequate chemical stability, excellent luminescence performance, and low thermal quenching property.[1,2] It is generally believed that $CaAlSiN_3:Eu^{2+}$ requires rigorous synthesis process such as high firing temperature and nitrogen pressure. Consequently, ensuing investigations have dealt with the synthesis for $CaAlSiN_3:Eu^{2+}$ along with detailed structure refinement analysis.[1-12] Up to now, a wide range of preparation methods have been reported: solid state reaction of binary nitrides;[1,6] gas reduction and nitridation of oxides;[13] carbothermal reduction nitridation of oxides, carbonates and carbon;[14-16] and self-propagating high-temperature synthesis,[4] spark plasma sintering,[17,18] direct nitridation,[9,19,20] and ammonothermal synthesis[3,5,21,22] from CaAlSi and (or) other corresponding alloys. Among them, solid state reaction can produce phosphor particles with good crystallinity, large size, and excellent luminescence. Moreover, this method is mostly suitable for mass production of the

nitride phosphor.

The solid state reaction preparation typically involves with four typical steps: (1) diffusion at interfaces of solid particles; (2) chemical reaction at atomic levels; (3) nucleation; and (4) material transportation and growth of nuclei. The raw materials play a key role in both diffusion and reaction steps. For instance, the Ca-α-sialon materials prepared from the $CaO-AlN-Si_3N_4$ system are formed through the well-known dissolution-diffusion-precipitation mechanism that requires a certain amount of liquid phase.[23-27] The liquid phase is from the eutectic reaction of CaO, SiO_2, and Al_2O_3, of which SiO_2 and Al_2O_3 are from the oxidized surface of the nitride starting powders. The reaction process is enhanced because diffusion distance among the reactants has been shortened in the liquid phase. The Ca-α-sialon product finally precipitates from the saturated liquid phase, and grows at the expense of dissolving silicon nitride and aluminum nitride raw materials. This inspires us that we can introduce some CaO to the $Ca_3N_2-AlN-Si_3N_4$ system to increase the amount of transient liquid phase during the formation of $CaAlSiN_3$ phase. Meanwhile, it is of considerable interest to know whether the benefits of more liquid phase could be extended to the synthesis of $CaAlSiN_3$ phosphor.

On the other hand, the unique structure of $CaAlSiN_3$, random distribution of Si and Al ions together with a partial replacement of N ions by O impurities at an identical crystallographic site, leads to inhomogeneous broadening emission.[28-31] The rather

broad emission band (full-width at half-maximum (FWHM): 90 ~ 105 nm) of $CaAlSiN_3:Eu^{2+}$ phosphors in the red-emission wavelength range greatly limits the maximum achievable luminous efficacy of high-quality white LEDs. In order to obtain a narrower emission band, the molar ratio of Al/Si in the raw materials was fixed to be 1:1 ($AlN : Si_3N_4 = 3:1$) instead of less than 1:1, and excess initial Ca content was added to compensate for the deficiency of Ca element, which originates from the volatilization of Ca source at high temperature, the deviation of Al/Si ratio from 1:1, and the partial replacement of N by O. Besides, it is indispensable to study whether the introduction of CaO will lead to the broadening luminescence by incorporating O ions into the lattice.

In the present study, $CaCO_3$ (decomposition into CaO at about 850 °C) was introduced to the conventional Ca_3N_2-AlN-Si_3N_4 system to act as partial Ca source. The effects of partial substitution for Ca_3N_2 by $CaCO_3$ on the crystallinity, cationic content, and luminescence property of the phosphor products were investigated. Besides, narrower emission band was obtained by compensating for the deficiency of Ca element with excess initial Ca content. Finally, the as-prepared $CaAlSiN_3:Eu^{2+}$ powders with narrower emission band were applied to excellent color-rendition warm white LEDs, showing improved luminous efficiency.

2 Experimental

2.1 Materials and synthesis

Eu^{2+} doped $CaAlSiN_3$ phosphors with the nominal composition of $Ca_{0.98}Eu_{0.02}AlSiN_3$

were synthesized by the solid state reaction method. The stoichiometric amounts of $CaCO_3$ (99.99%), Ca_3N_2 (Cerac, 99%), AlN (Tokuyama, H-Grade), α-Si_3N_4 (UBE, E-10), and Eu_2O_3 (99.99%) were mixed and ground in a Si_3N_4 mortar within a dried nitrogen filled glovebox. Thereafter, the powder mixture was transferred into a molybdenum boat in a horizontal tube furnace to conduct the vacuuming process, which was firstly carried out to the degree of -0.1 MPa; then, the process was repeated for another two times after filling the tube cavity with pure nitrogen. After that, the raw materials in the furnace were heated at 1600 °C for 4 h under a reducing atmosphere of 200 mL min^{-1} N_2 (99.999%) - 20 mL min^{-1} H_2 (99.999%) gas mixture. Finally, the as-prepared products were cooled down to room temperature and then ground finely to get the final products.

2.2 Materials characterization

The phase compositions were determined by X-ray diffraction (BrukerD8 Advanced, Germany) with Cu $K\alpha_1$ radiation ($\lambda = 0.15406$ nm) at 40 kV and 40 mA. A step size of 0.02° was used with a scan speed of 1°/min. Scanning electron micrographs (SEM) together with energy-dispersed X-ray spectroscopy (EDS) measurements were performed on a field-emission scanning electron microscope (Hitachi S-4800, Japan). The cationic compositions of the samples were analyzed by inductively coupled plasma atomic emission spectrometry (ICP-AES, Vista AX, Varian, USA). X-ray photoelectron spectroscopy (XPS) spectra were carried out with the X-ray photoelectron spectrometer (ESCALAB 250, Thermo Fisher Scientific, UK) using Al $K\alpha$ radiation at 15 kV and 10

mA. The photoluminescence spectra were measured by fluorescence spectrophotometer (Fluoromax-4, Jobin Yvon, France) equipped with a 150 W Xe lamp. For the temperature-dependent photoluminescence measurement, the powder sample was loaded in a sample cavity, and then heated to the test temperature by a high-temperature fluorescence controller (Tianjin Orient KOJI Co., LTD., TAP-02, China). The decay curves were measured using a Fluorescence Spectrophotometer (FLS980, Edinburgh, UK) with an excitation wavelength of 400 nm at room temperature. The optical properties of as-fabricated white LEDs were investigated by a high accuracy array spectroradiometer (HAAS-2000, EVERFINE, China) under a forward-bias current of 120 mA at room temperature in the Beijing YJXG photoelectric technology Co., Ltd.

3 Results and discussion

3.1 Addition of CaCO$_3$ into the Ca$_3$N$_2$-AlN-Si$_3$N$_4$ system

3.1.1 Phases analysis

To investigate the effects of CaO on the formation of CaAlSiN$_3$ phase in the Ca$_3$N$_2$-AlN-Si$_3$N$_4$ system, CaCO$_3$, which will decompose into CaO at ~ 850 °C, was partly added as calcium source together with Ca$_3$N$_2$. As the calcium source supplied by Ca$_3$N$_2$ is three times as much as that of CaCO$_3$ at the identical molar quantity, the molar ratios of CaCO$_3$/3Ca$_3$N$_2$ raw materials were designed to be 0:10, 1:9, 2:8, 3:7, 4:6, and 5:5 and the corresponding samples were labelled as C10N10O0, C10N9O1, C10N8O2, C10N7O3, C10N6O4, and C10N5O5, respectively. Therefore, the calcium source

percentages provided by $CaCO_3$ were 0, 10%, 20%, 30%, 40%, 50% for the samples, respectively, and meanwhile those provided by Ca_3N_2 were 100%, 90%, 80%, 70%, 60%, 50% for the samples, respectively. Fig. 1 displays the XRD patterns of the samples from C10N10O0 to C10N5O5. For all the samples, there exists the $CaAlSiN_3$ main phase (ICSD#161796) together with an impurity phase of AlN (PDF#25-1133). Probably due to the lower solubility of AlN in $CaAlSiN_3$, it has been proposed that Al/Si ions in $CaAlSiN_3$ structure occupy the identical 8b site in a disordered way with a ratio less than 1/1.[6] Therefore, a small amount of AlN is often detected as an impurity phase in the stoichiometric composition of $CaAlSiN_3$ product. Based on our previous research, AlN impurity could be eliminated through decreasing the Al/Si ratio in the raw materials,[28] and meanwhile the emission spectra become broader. In order to obtain a narrower emission, the Al/Si ratio in the raw materials was fixed to be 1:1 in this study. It has been found that in comparison with C10N10O0, C10N9O1 possesses higher diffraction intensity, indicating better crystallinity. At the same time, for the samples from C10N8O2 to C10N5O5, the diffraction intensity of $CaAlSiN_3$ main phase decreases, while that of the minor AlN impurity increases. For the samples with more residual AlN impurity, the Al/Si ratio in the $CaAlSiN_3$ main phase is deviating larger from 1:1. And the composition variation of Al/Si ratio in the $CaAlSiN_3$ main phase may mainly accounts for the relative intensity change for the peaks at ~35.5 and ~36.5 degrees. [14,31]
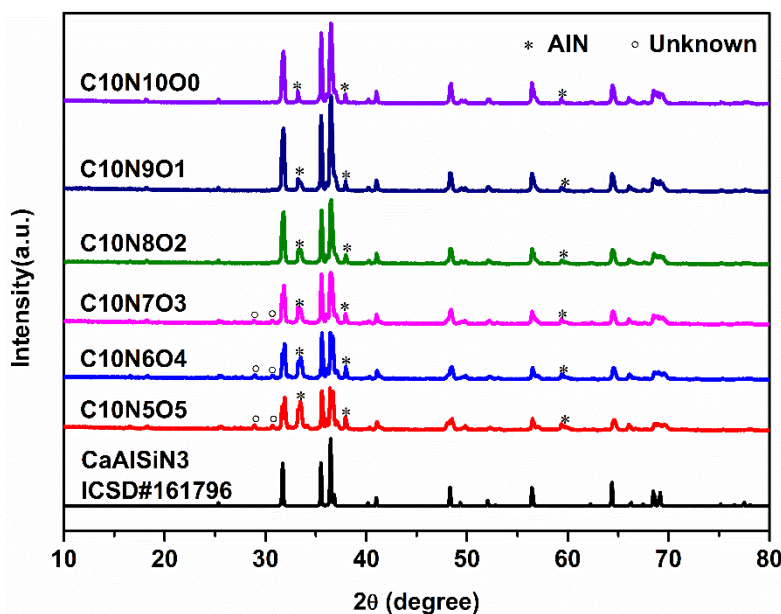
Fig. 1 XRD patterns of the samples from C10N10O0 to C10N5O5.

3.1.2 Morphology

Fig. 2 shows the SEM micrographs of the samples from C10N10O0 to C10N7O3. The cleavage planes of individual particles in the sample C10N10O0 are not clear, and the other particles adhere to their surfaces. However, with the addition of $CaCO_3$ (samples C10N9O1 to C10N7O3), the surfaces of such cleavage planes become much more smooth and clear. Particularly for the sample C10N9O1, the particles are well-faceted and show the nature of individual crystallite, suggesting better crystallinity. It can also be understood from the XRD patterns that the peaks of the sample C10N9O1 are higher than those of the sample C10N10O0. Unlike the sample C10N10O0 using only Ca_3N_2 as the calcium source, the samples with the addition of $CaCO_3$ own two sources for transient liquid formations: One is the eutectic reaction of SiO_2, Al_2O_3, Eu_2O_3, and CaO (decomposed from $CaCO_3$), among which SiO_2 and Al_2O_3 are from the surface of the nitride starting powders (AlN and Si_3N_4); the other is the melting of Ca_3N_2. According

to the $CaO-SiO_2-Al_2O_3$ phase diagram,[32] the oxide liquid begins to form at a eutectic temperature of 1170 °C. It is therefore reasonable to conclude that the $CaO-SiO_2-Al_2O_3-Eu_2O_3$ quaternary system have much lower eutectic temperature than 1170 °C. In contrast, without the addition of $CaCO_3$, a transient liquid phase is produced as a result of the melting of Ca_3N_2 at a slightly higher temperature (>1195 °C).[33] With the addition of $CaCO_3$, once the eutectic oxide liquid forms, it wets $\alpha-Si_3N_4$ first, and then dissolves AlN and $\alpha-Si_3N_4$, leading to the increased nitrogen concentration in the liquid, $CaAlSiN_3$ finally precipitates. By comparison, without the addition of $CaCO_3$, a nitrogen-rich liquid is produced due to the melting of Ca_3N_2. Therefore, the dissolution of AlN and $\alpha-Si_3N_4$ into this nitride liquid is expected to be suppressed. As a consequence, the sample C10N9O1 owns better crystallinity than C10N10O0. Nevertheless, as for the samples C10N8O2 and C10N7O3, the transient liquid phases will possess a higher oxygen and lower nitrogen concentration with increasing amount of $CaCO_3$, leading to a weak precipitation of the $CaAlSiN_3$ main phase. In general, the $CaAlSiN_3:Eu^{2+}$ materials in our study are formed through the well-known dissolution-diffusion-precipitation mechanism. It has also been found from the SEM images that besides the big particles, uniform small sphere particles are formed, and the amounts of small ones are gradually increasing from C10N10O0 to C10N7O3. The EDS results (as shown in Fig. 3) suggest that the element compositions of the small particles (Fig. 3a) and the big particles (Fig. 3b) are mainly AlN and $CaAlSiN_3$, respectively. This is in accordance with the results from the XRD patterns that the peaks of AlN are becoming higher, and the ones of $CaAlSiN_3$ are getting lower with the increasing amount of

CaCO₃. Hence, we draw the conclusion that the crystallinity has been improved with

10% Ca source provided by CaCO₃ rather than all from Ca₃N₂.
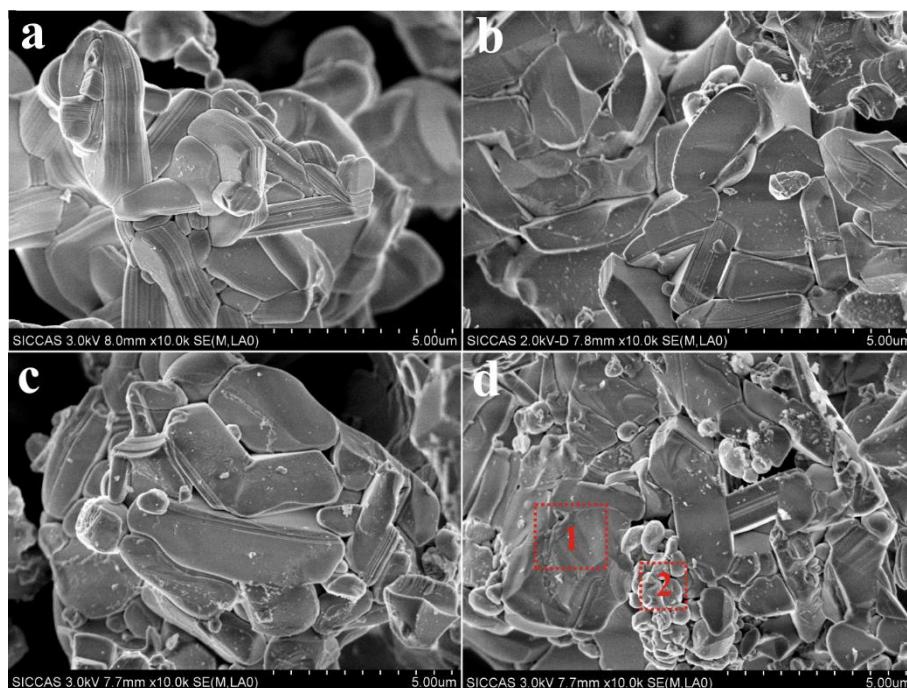
Fig. 2 SEM images of the samples (a) C10N10O0, (b) C10N9O1, (c) C10N8O2, and

(d) C10N7O3.
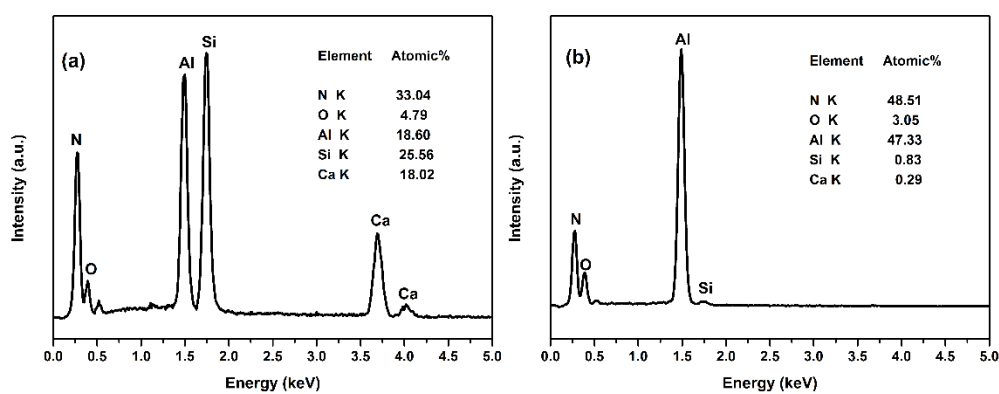
Fig. 3 EDS measurement results of the area 1 (a) and the area 2 (b) in the Fig 2d.

3.1.3 Chemical composition analysis

Table 1 reports the analyzed cationic ratios of the samples from C10N10O0 to C10N5O5. The deficiency of Ca/Eu component in comparison with the theoretical value is mainly attributed to their evaporation at high temperature.[4,13] The Al and Si elements show no obvious change, while both the Ca and Eu contents present a progressively upward trend. As all the Ca/Eu ions have entered into the liquid at high temperature, with the increase of $CaCO_3$ amount, more transient liquid phase forms, thus the concentration of liquid Ca/Eu decreases, leading to the reduction of their equilibrium pressure of gaseous Ca/Eu, and therefore the weak evaporation.

Table 1 Analyzed cationic ratios of the samples from C10N10O0 to C10N5O5.

Samples	Initial composition				Final composition[a]			
	Ca	Eu	Al	Si	Ca	Eu	Al	Si
C10N10O0	0.98	0.02	1.00	1.00	0.824(9)	0.008(7)	0.994(2)	1.005(8)
C10N9O1	0.98	0.02	1.00	1.00	0.837(0)	0.010(6)	0.986(6)	1.013(4)
C10N8O2	0.98	0.02	1.00	1.00	0.856(8)	0.012(1)	0.977(1)	1.022(9)
C10N7O3	0.98	0.02	1.00	1.00	0.876(2)	0.013(0)	0.987(7)	1.012(3)
C10N6O4	0.98	0.02	1.00	1.00	0.896(5)	0.014(8)	0.992(2)	1.007(8)
C10N5O5	0.98	0.02	1.00	1.00	0.891(5)	0.014(6)	0.989(4)	1.010(6)

[a]Normalized against the total Al + Si = 2.

3.1.4 XPS analysis

The surface states of the phosphors are also investigated by XPS analysis. Fig. 4a presents the high resolution XPS spectra of Ca 2p for samples from C10N10O0 to

C10N7O3, and the corresponding deconvoluted spectra are shown in Fig. 4b ~ e, with the experimental spectra depicted with dots and the simulated one with solid lines. Compared with the Ca 2p of C10N10O0, the other three spectra shift to the lower energy side, and in particular the Ca 2p of C10N9O1 gives a broader band. The bonding energy of Ca-O is higher than that of Ca-N due to the greater electronegativity of oxygen.[34] In our case, Ca $2p_{1/2}$ can be deconvoluted into Ca-O ($2p_{1/2}$) and Ca-N ($2p_{1/2}$) at ~ 351.01 and ~ 349.79 eV, respectively, and Ca $2p_{3/2}$ into Ca-O ($2p_{3/2}$) and Ca-N ($2p_{3/2}$) at ~ 347.52 and ~ 346.37 eV, respectively. As can be seen, C10N9O1 possesses the highest Ca-N binding relative intensity, while the other three samples show little difference. Similar results are observed in the Si 2p and Al 2p cases that C10N9O1 possesses the highest Al-N and Si-N binding relative intensity. Whereas, Al-N and Si-N binding relative intensity become a little lower for samples of C10N8O2 and C10N7O3 compared with C10N10O0 as shown in Fig. S1 and S2 (Supporting Information). It means that the introduction of CaO may not incorporate O ion into the lattice matrix of $CaAlSiN_3$ as for C10N9O1. On the contrary, C10N9O1 owns a better nitridation degree than C10N10O0 on the surface of the phosphors. With regard to C10N8O2 and C10N7O3, O ions may partially enter into the host lattice of $CaAlSiN_3$, yet it makes little difference for the bonding of Ca ions.
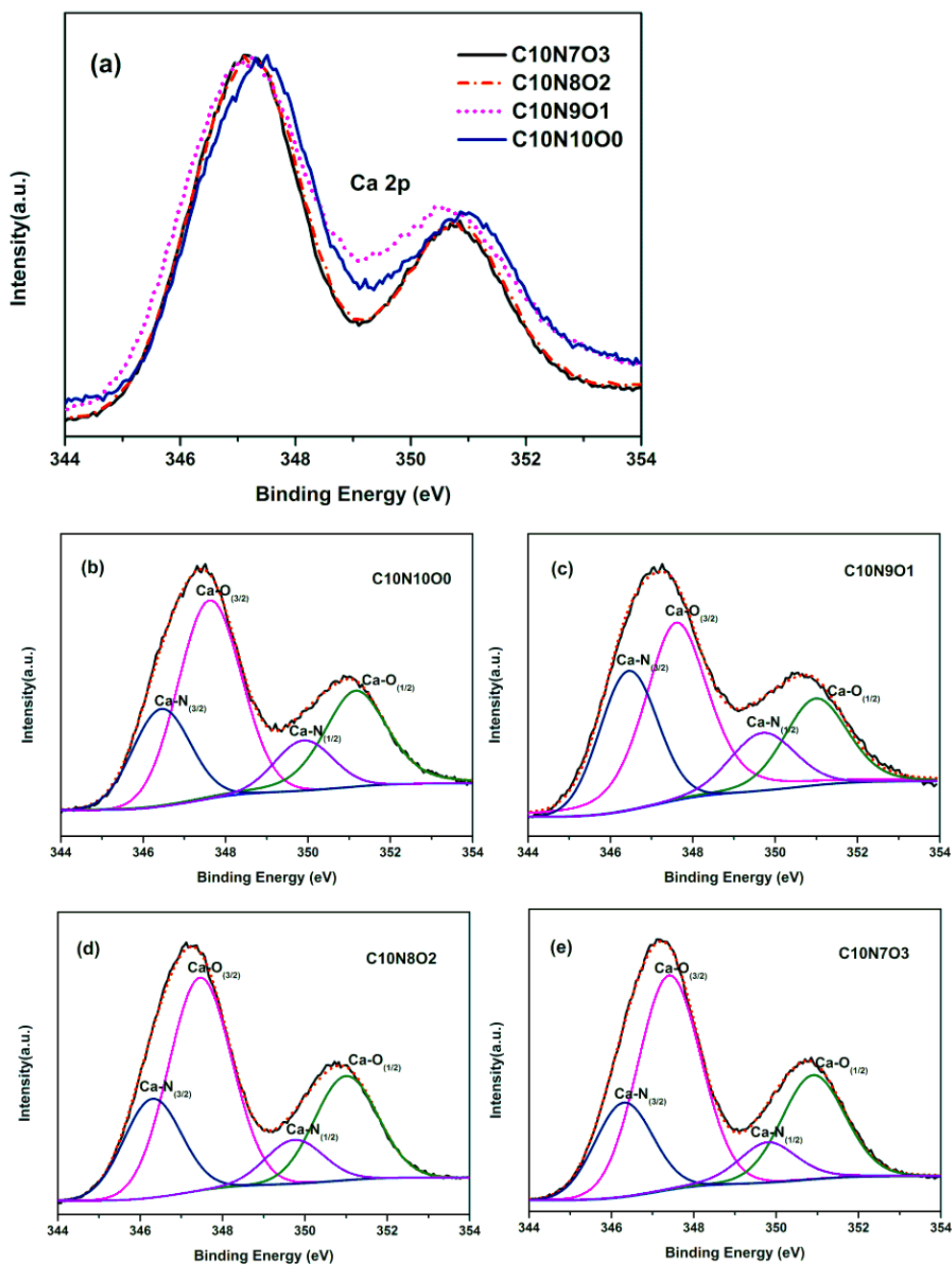
Fig. 4 XPS spectra of Ca 2p for samples from C10N10O0 to C10N7O3 (a), and the deconvoluted spectra of C10N10O0 (b), C10N9O1 (c), C10N8O2 (d), and C10N7O3 (e) after 10s Ar gas purge, with the experimental spectra depicted with dots and the simulated one with solid lines. All spectra were calibrated with C 1s peak.

3.1.5 Photoluminescence measurements

Fig. 5 presents the photoluminescence excitation and emission spectra of the samples from C10N10O0 to C10N5O5. Each phosphor shows a broad excitation spectra from 250 to 600 nm, matching effectively with UV (~ 380 nm) and (or) blue (~ 450 nm) LED chips. The broad excitation bands for all samples are assigned to the allowed $4f^7 \rightarrow 4f^65d^1$ transition of Eu^{2+} ions. The $5d$ levels of Eu^{2+} ions that are not shielded completely by the outer environment will split under various ligand field strength, and the number of split levels is determined by the local symmetry around the Eu^{2+} ions. According to the symmetry of nitrogen ion around the Eu^{2+} ion which is located at the Ca^{2+} site, the $5d$ orbitals of Eu^{2+} are inclined to be divided to two crystal field components. And the two broad peaks observed in the broad excitation band can be ascribed to the transitions from $4f$ to each crystal field component.[1,4] The strong red emission spectra centered at ~ 630 nm are attributed to the characteristic $4f^65d^1 \rightarrow 4f^7$ transition of Eu^{2+} ions. Table 2 summarizes the FWHM, peaking emission wavelength, and peaking emission intensity for the corresponding emission spectra. The sample of C10N9O1 gives a narrower FWHM, enhanced emission intensity, and a small red-shift emission compared with C10N10O0, which can be attributed to its better nitridation as revealed by the XPS results. Additionally, the emission spectra show a gradual blue-shift and broadening for the samples from C10N7O3 to C10N5O5, which will be discussed in the following part. And the blue-shift emission could be partially ascribed to the fact that the crystal-field splitting becomes smaller with substitution for N by O ions at an identical crystallographic site in the host lattice.[28]
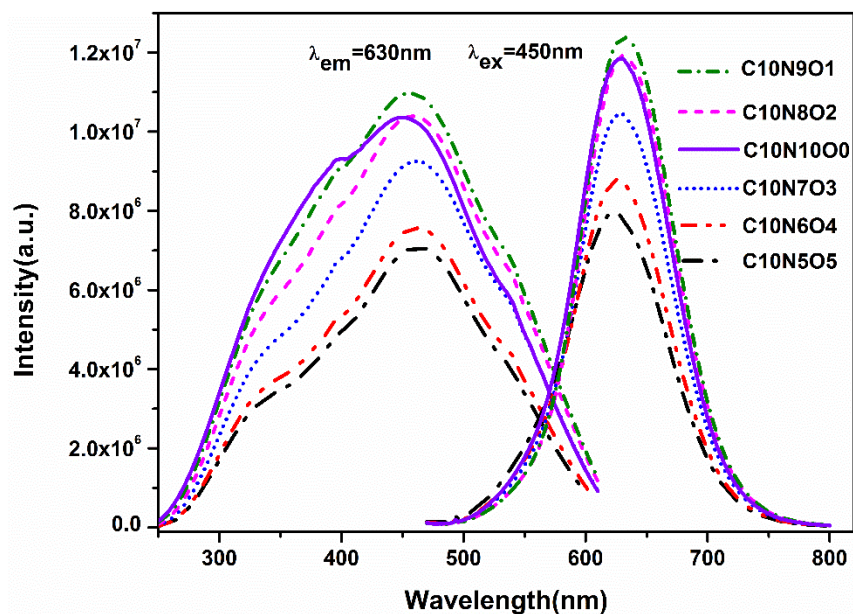
Fig. 5 Photoluminescence spectra of the samples from C10N10O0 to C10N5O5.

Table 2 FWHM, peaking emission wavelength, and peaking emission intensity of

the samples from C10N10O0 to C10N5O5.

Sample	FWHM (nm)	Peak position (nm)	Peak intensity (a.u.)
C10N10O0	90	630	1.18485×10^7
C10N9O1	88	632	1.23946×10^7
C10N8O2	88	630	1.19191×10^7
C10N7O3	90	627	1.0463×10^7
C10N6O4	92	627	8.79937×10^6
C1ON5O5	97	625	7.96675×10^6

3.1.6 Decay behavior

Fig. 6 depicts the decay curves monitored at 550 nm and 700 nm for the samples of C10N10O0, C10N7O3, and C10N5O5, respectively. The difference between the decay rate at 550 nm and 700 nm is ascribed to the nonradiative energy transfer. The decay curves monitored at 550 nm show faster nonexponential forms, on behalf the donor decay. By contrast, the decay curves monitored at 700 nm representative of the acceptor decay exhibit almost single-exponential radiative decay rate. Both an inhomogeneous distribution of Al/Si and a partial replacement of N by O around the Eu^{2+} activators contribute to the energy transfer.[29,35] With the increasing amount of $CaCO_3$, the Al/Si ratios in the $CaAlSiN_3$ host decrease because the residual minor AlN phase increases as shown in the XRD patterns and SEM images, and the N/O ratios also decreases slightly due to the incorporation of a few O ions as indicated by the XPS results. As can be seen from Fig. 6, the donor decay slows with the decrease of Al/Si and N/O ratios, which is in accordance with the previous research results.[31,35] Compared with C10N5O5, the high-energy side (550 nm) of C10N10O0 decays much faster, that is to say, the energy transfer occurs strongly from high-energy site to the low-energy one, thus leading to the decline of high-energy emission and the simultaneous increasing of low-energy emission. The active energy transfer eventually controls the final spectral distribution. Therefore, it is easy to understand that C10N10O0 possesses a narrower and red-shift emission. That is to say, the inhomogeneous broadening along with the blue-shift emission of C10N7O3 and C10N5O5 could be associated with the decrease of energy transfer rate.
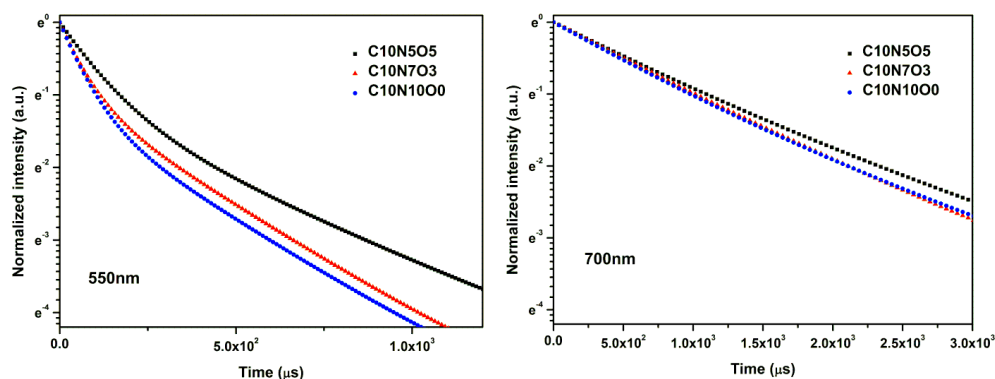
Fig. 6 Decay curves for the samples of C10N10O0, C10N7O3, and C10N5O5

monitored at 550 nm and 700 nm, respectively.

3.2 Benefits of excess Ca initial content on the photoluminescence properties

The deficiency of initial calcium (as shown in Table 1) is observed for the stoichiometric starting composition which is mainly caused by the evaporation at high temperature. The partial substitution of Ca_3N_2 by $CaCO_3$ could suppress the evaporation of calcium to some extent. In order to effectively compensate for the calcium deficiency, excess initial calcium is introduced while keeping the ratio of $CaCO_3/3Ca_3N_2 = 1:9$ to be constant. The total amount of initial calcium content is 110%, 120%, 130%, 140%, and 160% compared with the stoichiometric one (100%), and the corresponding samples are identified as C11N9O1, C12N9O1, C13N9O1, C14N9O1, and C16N9O1, respectively. The XRD patterns of the samples from C11N9O1 to C16N9O1 are shown in Fig. 7. Generally, the XRD patterns show no obvious change except for the sample of C16N9O1. Impurity CaO phase appears for C16N9O1, indicating the excess of calcium source. According to Table 3, the initial content of Ca source required to compensate for the deficiency is found to be as much as 1.4 times (sample C14N9O1) of the stoichiometric quantity (sample C10N9O1). However, not only is the evaporation

at high temperature responsible for the deficiency, the deviation of Al/Si from 1:1 and the partial replacement of N by O also contribute to the deficiency of Ca element. Thus, it is almost impossible for the Ca content to achieve the stoichiometric value.
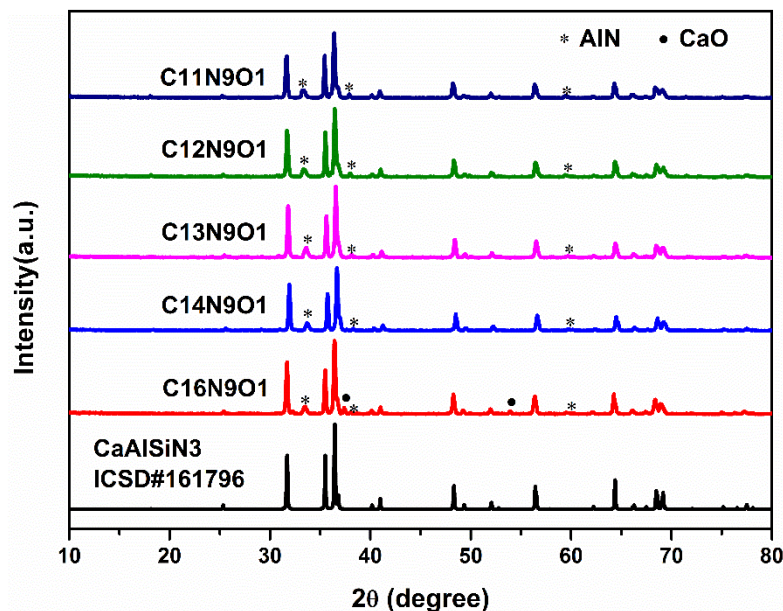
Fig. 7 XRD patterns of the samples from C11N9O1 to C16N9O1.

Table 3. Analyzed cationic ratios of the samples from C11N9O1 to C16N9O1.

Sample	Initial composition			Final composition[b]		
	Ca	Al	Si	Ca	Al	Si
C10N9O1	0.98	1.00	1.00	0.837(0)	0.986(6)	1.013(4)
C11N9O1	1.078	1.00	1.00	0.876(4)	1.012(4)	0.987(6)
C12N9O1	1.176	1.00	1.00	0.901(7)	1.059(6)	0.940(4)
C13N9O1	1.274	1.00	1.00	0.949(6)	1.020(1)	0.979(9)
C14N9O1	1.372	1.00	1.00	0.978(9)	1.020(1)	0.979(9)
C16N9O1	1.568	1.00	1.00	1.058(1)	1.036(6)	0.963(4)

[b]Normalized against the total Al + Si = 2.

Fig. 8 exhibits the photoluminescence spectra with different initial Ca contents and the corresponding information about the emission spectra is listed in Table 4. As shown in Fig. 8 and Table 4, the peaking emission wavelength shows a small fluctuation by increasing the initial Ca content, and the peaking emission intensity is maximized at the initial Ca content of 110%. Additionally, the FWHMs become narrower and narrower with increment of calcium content. On the basis of our previous work, ion vacancy V_{Ca} together with the substitutional O_N will be induced due to the deficiency of calcium. With the increase of Ca content, the abovementioned defects will be decreased. Therefore, less potential killer sites will be located nearby the Eu^{2+} activators, resulting in a faster decay rate (as shown in Fig. 9). This to some extent explains the narrower emission band.
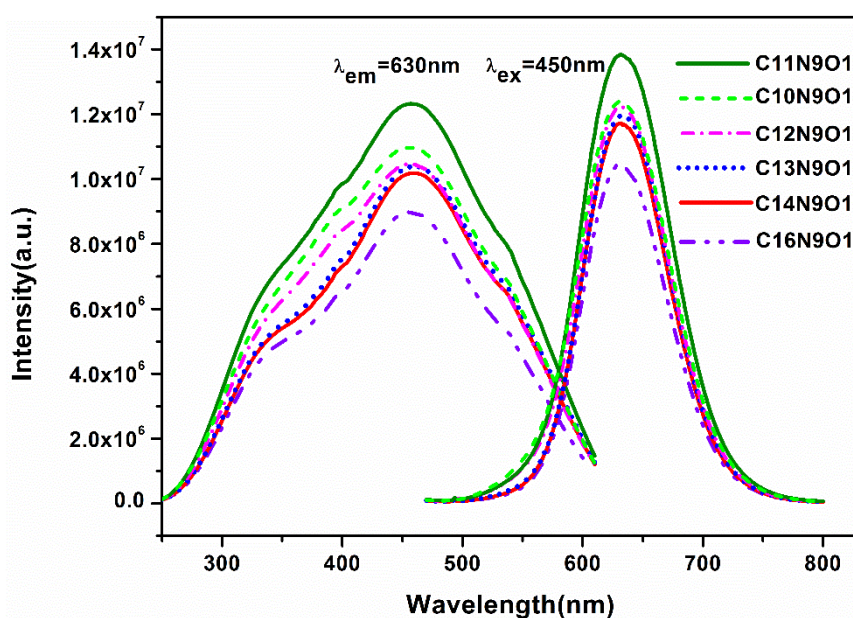
Fig. 8 Photoluminescence spectra of the samples from C11N9O1 to C16N9O1.

Table 4 FWHM, peaking emission wavelength, and peaking emission intensity of

the samples from C11N9O1 to C16N9O1.

Sample	FWHM (nm)	Peak position (nm)	Peak intensity (a.u.)
C10N9O1	88	632	1.23946×10^7
C11N9O1	87	632	1.3838×10^7
C12N9O1	86	630	1.22647×10^7
C13N9O1	84	631	1.19477×10^7
C14N9O1	83	632	1.17283×10^7
C16N9O1	82	630	1.04758×10^7
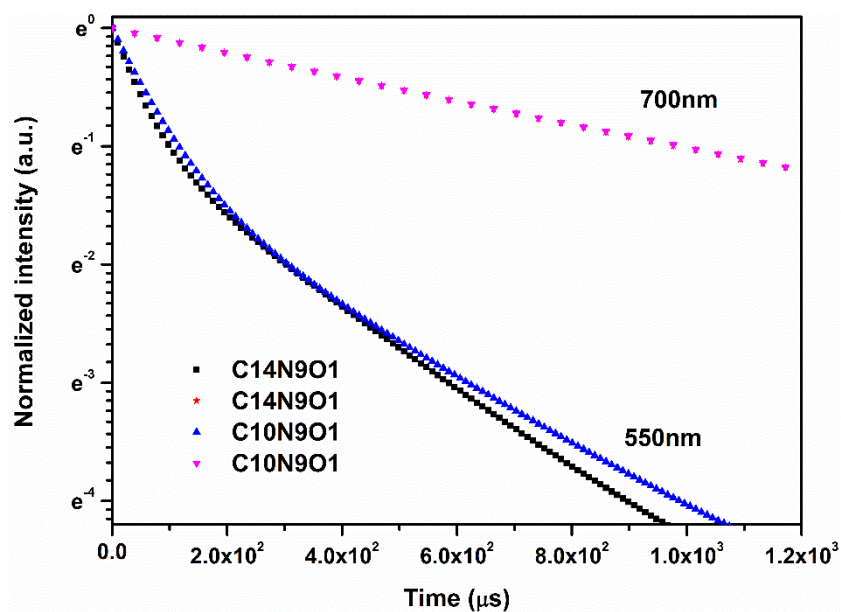
Fig. 9 Decay curves for the samples of C10N9O1 and C14N9O1 monitored at

550 nm and 700 nm, respectively.

3.3 Thermal stability

For white LED applications, thermal stability is an important technological parameter

for maintaining the stability of the chromaticity and the brightness of white light output

at high temperature (~150 °C). We have measured temperature-dependent

luminescence spectra for samples of C10N10O0, C10N9O1, and C14N9O1 from 25 ℃

to 200 ℃, as shown in Fig. 10. It is clearly seen that all the compounds exhibit small

thermal quenching. In particular, at 200 ℃, the emission intensity remains 87%, 91%,

and 95% of the initial intensity at 25 ℃ for C10N10O0, C10N9O1, and C14N9O1,

respectively. And the better thermal stability of C10N9O1 than C10N10O0 may be

ascribed to the higher nitridation on the surface of the compound as reveled by the XPS

results.
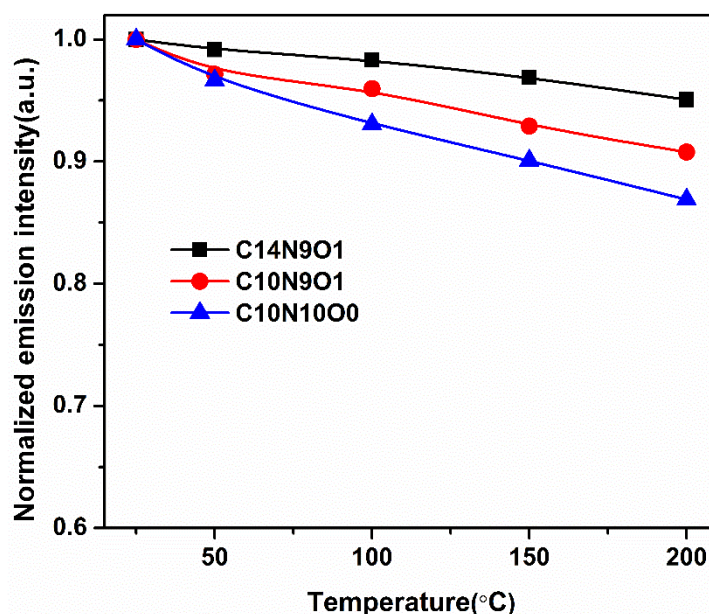
Fig. 10. Temperature dependence of the normalized emission intensity for samples of

C10N10O0, C10N9O1, and C14N9O1, respectively.

3.4 Application evaluation of the phosphors in White LEDs

The practical performance of as-synthesized $CaAlSiN_3:Eu^{2+}$ red-emitting phosphors in

solid-state lighting applications is evaluated by the fabrication of trichromatic warm-white LEDs together with blue-emitting LED chips (457.5 ~ 460 nm) and green-emitting phosphors (ZYP520G2, Beijing Nakamura-Yuji Science and Technology Co., Ltd.) at a correlated color temperature (CCT) of 3000 K. The electroluminescence spectra of the fabricated white LEDs using C10N10O0 and C14N9O1 samples are illustrated in Fig. 11, and the relevant color rendering properties of the white LEDs using C10N10O0, C10N9O1, C11N9O1, and C14N9O1 samples are summarized in Table 5. Compared with the C10N10O0 based white LED, the LED consisting of C14N9O1 with narrower band shows a 15% increased luminous efficacy (from 73 to 86 lm/W) under a forward-bias current of 120 mA. This is because that the sensitivity curve of the human eye is very steep in the saturated red spectral range, thus even small changes in emission peak position and width have a great impact on the spectral lumen equivalent.[36] All the LED systems using the synthesized samples together with the commercial green-emitting ZYP520G2 phosphor attain excellent color rendition with the high general color rendering index (CRI) Ra value of 97.5-98, as well as the special CRIs R_9 (strong red) of 98.5-98.9, R_{13} (skin tone of European women) of 98.2-99, and R_{15} (skin tone of Asian women) of 97.4-97.8. These results were satisfactory to meet the requirements for high-color-rendition general lighting, indicating the excellent performance of the as-prepared phosphors.
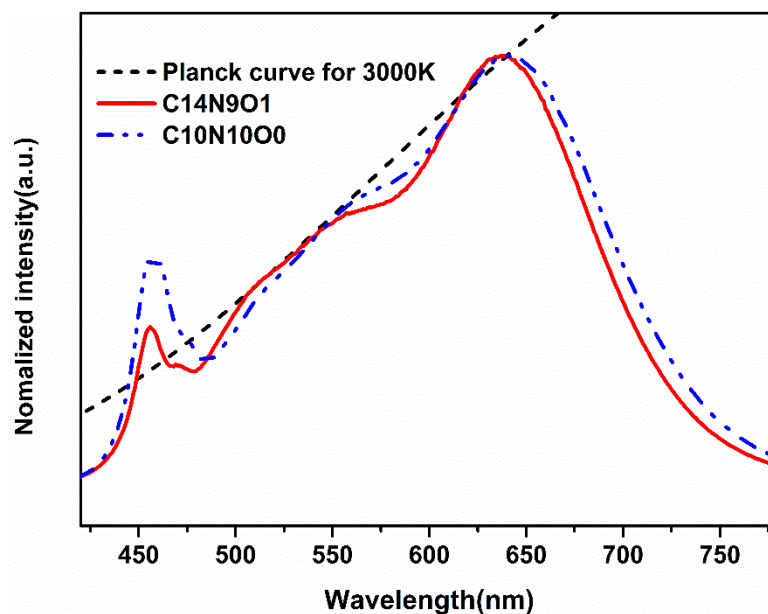
Fig. 11 Normalized electroluminescence spectra of the white LEDs fabricated by

using C10N10O0 and C14N9O1 as red component, respectively, operated at a

forward-bias current of 120 mA at room temperature

Table 5 CRI and luminous efficacy of white LEDs fabricated using the as-prepared

$CaAlSiN_3:Eu^{2+}$ phosphors

Red-emitting phosphor sample	CRIs				Luminous efficacy (lm/W)
	Ra	R9	R13	R15	
C10N10O0	98	98.5	98.2	97.8	73
C10N9O1	98	98.9	98.6	97.8	82
C11N9O1	98	98.7	99	97.8	83
C14N9O1	97.5	98.7	98.5	97.4	86

4 Conclusions

In summary, the influence of $CaCO_3$ on the solid state reaction and photoluminescence properties of the red-emitting phosphor $CaAlSiN_3:Eu^{2+}$ has been investigated. At the optimal amount of $CaCO_3$, improved crystallinity and surface nitridation were obtained. More transient liquid phase formed and less Ca/Eu evaporated with the amount of $CaCO_3$ increasing. By adding excess initial Ca content, narrower emission band was acquired together with faster decay rate due to less potential killer sites such as V_{Ca}, O_N defects. The narrower emission band favorably resulted in an increase of 15% in luminous efficacy with an excellent high-color-rendition index of the fabricated white LED.

Acknowledgement

References

1 K. Uheda, N. Hirosaki, and H. Yamamoto, *Phys. Stat. Sol. (A),* 2006, 203, 2712-2717.

2 K. Uheda, N. Hirosaki, Y. Yamamoto, A. Naito, T. Nakajima, and H. Yamamoto, *Electrochem. Sol. Stat. Lett.,* 2006, 9, H22-H25.

3 J. W. Li, T. Watanabe, H. Wada, T. Setoyama, and M. Yoshimura, *Chem. Mater.,* 2007, 19, 3592-3594.

4 X. Q. Piao, K. Machida, T. Horikawa, H. Hanzawa, Y. Shimomura, and N. Kijima, *Chem. Mater.,* 2007, 19, 4592-4599.

5 J. W. Li, T. Watanabe, N. Sakamoto, H. Wada, T. Setoyama, and M. Yoshimura, *Chem. Mater.,* 2008, 20, 2095-2105.

6 Y. Q. Li, N. Hirosaki, R. J. Xie, T. Takeda, and M. Mitomo, *Chem. Mater.,* 2008, 20, 6704-6714.

7 H. Watanabe, H. Yamane, and N. Kijima, *J. Sol. Stat. Chem.,* 2008, 181, 1848-1852.

8 K. Uheda, H. Yamamoto, H. Yamane, W. Inami, K. Tsuda, Y. Yamamoto, and N. Hirosaki, *J. Ceram. Soc. Jp.,* 2009, 117, 94-99.

9 H. Watanabe, M. Imai, and N. Kijima, *J. Am. Ceram. Soc.,* 2009, 92, 641-648.

10 D. Urushihara, T. Asaka, T. Takeda, N. Hirosaki, and K. Fukuda, *Powder Diffr.,* 2011, 26, S38-S43.

11 B. Dierre, T. Takeda, T. Sekiguchi, T. Suehiro, K. Takahashi, Y. Yamamoto, R. J. Xie, and N. Hirosaki, *Sci. Technol. Adv. Mater.,* 2013, 14, 064201.

12 J. Cho, B. K. Bang, S. J. Jeong, and C. H. Kim, *RSC Adv.,* 2014, 4, 23218-23222.

13 T. Suehiro, R. J. Xie, and N. Hirosaki, *Ind. Eng. Chem. Res.,* 2014, 53, 2713-2717.

14 S. X. Li, X. Peng, X. J. Liu, and Z. R. Huang, *Opt. Mater.,* 2014, 38, 242-247.

15 H. S. Kim, K. Machida, T. Horikawa, and H. Hanzawa, *Chem. Lett.*, 2014, 43, 533-534.

16 H. S. Kim, T. Horikawa, H. Hanzawa, and K. Machida, *J. Phys.*, 2012, 379, 012016.

17 H. Q. Trinh, J. O. Jo, S. B. Lee, and Y. S. Mok, *Curr. Appl. Phys.,* 2014, 14, 1051-1056.

18 Y. S. Kim, S. W. Choi, J. H. Park, E. Bok, B. K. Kim, and S. H. Hong, *Esc J. Sol. Stat. Sci. Technol.,* 2013, 2, R3021-R3025.

19 H. Watanabe, and N. Kijma, *J. Ceram. Soc. Jp.,* 2009, 117, 115-119.

20 J. J. Yang, T. Wang, D. C. Chen, G. D. Chen, and Q. L. Liu, *Mater. Sci. Eng. B,* 2012, 177, 1596-1604.

21 J. W. Li, T. Watanabe, H. Wada, T. Setoyama, and M. Yoshimura, *J. Am. Ceram. Soc.,* 2009, 92, 344-349.

22 T. Watanabe, K. Nonaka, J. W. Li, K. Kishida, M. Yoshimura, *J. Ceram. Soc. Jp.,* 2012, 120, 500-502.

23 Z. K. Huang, W. Y. Sun, and D. S. Yan, *J. Mater. Sci. Lett.,* 1985, 4, 255-259.

24 J. W. T. van Rutten, H. T. Hintzen, and R. Metselaar, *J. Eu. Ceram. Soc.,* 1996, 16, 995-999.

25 V. A. Izhevskiy, L. A. Genova, J. C. Bressiani, and F. Aldinger, *J. Eu. Ceram. Soc.,* 2000, 20, 2275-2295.

26 P. L. Wang, C. Zhang, W. Y. Sun, and D. S. Yan, *J. Eu. Ceram. Soc.,* 1999, 19, 553-560.

27 C. L. Hewett, Y. B. Cheng, B. C. Muddle, and M. B. Trigg, *J. Am. Ceram. Soc.,* 1998, 81, 1781-1788.

28 T. Wang, J. J. Yang, Y. D. Mo, L. Bian, Z. Song, and Q. L. Liu, *J. Lumin.,* 2013, 137, 173-179.

29 Y. W. Jung, B. Lee, S. P. Singh, and K. S. Sohn, *Opt. Express,* 2010, 18, 17805-17818.

30 S. Lee, and K. S. Sohn, *Opt. Lett.,* 2010, 35, 1004-1006.

31 S. X. Li, X. J. Liu, J. Q. Liu, H. L. Li, R. H. Mao, Z. R. Huang, and R. J. Xie, *J. Mater. Res.*, 2015, DOI: 10.1557/jmr.2015.125.

32 E. M. Levin, C. R. Robbins, and H. F. McMurdie, *Phase Diagrams for Ceramists*, ed. M. K. Reser, American Ceramic Society, Cleveland OH, USA, 1964.

33 J.E. Macintyre, and F. Macdonald, *Dictionary of Inorganic Compounds*, CRC Press, London, 1992.

34 J. Zhu, L. Wang, T. L. Zhou, Y. J. Cho, T. Suehiro, T. Takeda, M. Lu, T. Sekiguchi, N. Hirosakia, and R. J. Xie, *J. Mater. Chem. C*, 2015, 3 , 3181-3188.

35 T. Wang, P. Zheng, X. L. Liu, H. F. Chen, S. S. Yang, and Q. L. Liu, *J. Electrochem. Soc.,* 2013, 161, H25-H28.

36 P. Pust, V. Weiler, C. Hecht, A. Tücks, A. S. Wochnik, A-K. Henß, D. Wiechert, C. Scheu, P-J. Schmidt, and W. Schnick, *Nat. Mater.,* 2014, 13, 891-896.